

**PRACTICAL SUPERCONDUCTOR DEVELOPMENT**  
**FOR ELECTRICAL POWER APPLICATIONS**  
**ARGONNE NATIONAL LABORATORY**  
**QUARTERLY REPORT FOR THE PERIOD ENDING JUNE 30, 2003**

This is a multiyear experimental research program that focuses on improving relevant material properties of high-critical temperature ( $T_c$ ) superconductors and developing fabrication methods that can be transferred to industry for production of commercial conductors. The development of teaming relationships through agreements with industrial partners is a key element of the Argonne National Laboratory (ANL) program.

### **Technical Highlights**

A transport critical current density ( $J_c$ ) of  $1.2 \times 10^6$  A/cm<sup>2</sup> was measured with a sample made with the standard inclined substrate deposition (ISD) architecture. Recent results are described from a study of SrRuO<sub>3</sub> (SRO), a potential alternative buffer layer in coated conductors made by the inclined substrate deposition (ISD) method. Basic features of Raman microscopy are also discussed, and results are presented from a detailed Raman microprobe study of a 1.25-m-long YBCO coated conductor specimen produced at Oak Ridge National Laboratory (ORNL). Strain tolerance data are presented as a function of YBCO thickness for coated conductors with the standard ISD architecture.

#### YBCO Films on Standard ISD Architecture

The standard ISD architecture consists of YBCO/CeO<sub>2</sub>/yttria-stabilized zirconia (YSZ)/ISD MgO/Hastelloy C (HC). Details of the ISD method were described previously [1, 2]. During the last year, the biaxial texture of the YBCO layer was sharpened considerably by carefully optimizing the deposition parameters for the individual layers, decreasing the full-width at half maximum (FWHM) of the YBCO(103) pole from  $\approx 12^\circ$  on average to  $\approx 10^\circ$ . Along with the enhanced texture, YBCO films with the standard ISD architecture exhibited an increase in transport  $J_c$ . It is believed that the increase in  $J_c$  resulted from the improvement in YBCO texture. Figure 1 shows the results from transport measurements on a recent standard ISD sample with a transport  $J_c$  of  $1.2 \times 10^6$  A/cm<sup>2</sup>.

#### YBCO Films on SRO-Buffered ISD MgO Substrates

SRO is presently being investigated as a potential alternative buffer layer for ISD coated conductors, i.e., coated conductors made by the ISD method. SRO is chemically stable and exhibits good thermal and electrical conductivity. Its structure at room

temperature is orthorhombic, with lattice parameters  $a = 5.537\text{\AA}$ ,  $b = 7.852\text{\AA}$ , and  $c = 5.573\text{\AA}$  (JCPDS# 89-5713). Because of its relatively small lattice mismatch ( $\approx 6.5\%$ ) with MgO, SRO can be grown epitaxially on the MgO template layer, and because its lattice mismatch with YBCO is intermediate between that of YSZ and  $\text{CeO}_2$ , it might serve as a suitable alternative for one or both of the YSZ and  $\text{CeO}_2$  layers. We previously presented [2]  $T_c$  and  $J_c$  curves for an  $\approx 0.3\text{-}\mu\text{m}$ -thick YBCO film deposited on a SRO-buffered MgO single-crystal substrate. The curves revealed a sharp transition, with  $T_c$  (onset) of 91 K and a transport  $J_c$  of  $2.4 \times 10^6\text{ A/cm}^2$ , showing the good potential of SRO. In Ref. 2, we also reported a transport  $J_c$  of 30-100  $\text{kA/cm}^2$  for our first samples of YBCO deposited on SRO-buffered ISD MgO substrates. In this report, we describe recent results for coated conductors with the architecture: YBCO/SRO/ISD MgO/HC.

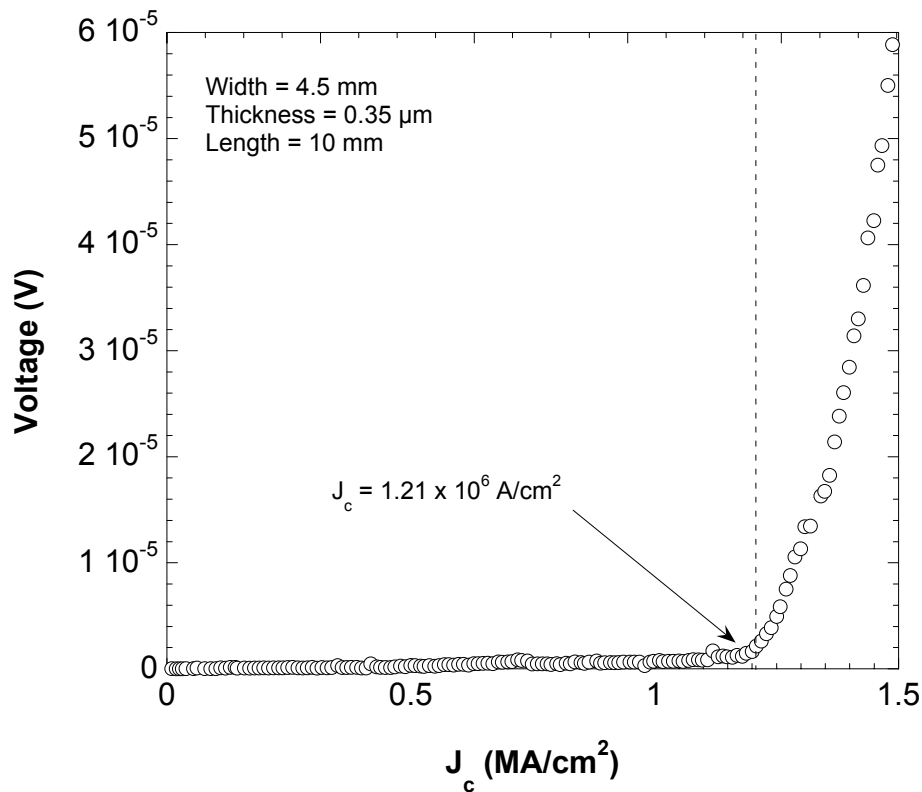


Fig. 1. Transport measurements from recent sample with standard ISD architecture, YBCO/ $\text{CeO}_2$ /yttria-stabilized zirconia (YSZ)/ISD MgO/Hastelloy C (HC).

HC substrates were mechanically polished to a mirror finish by using  $0.25\text{-}\mu\text{m}$  diamond paste. On the polished HC substrate, an ISD MgO film was deposited at an angle of  $55^\circ$  from the substrate normal by electron beam evaporation. On top of this ISD film, a homoepitaxial (HE) MgO layer was then deposited normal to the substrate. Hereafter in this report, the term ISD MgO refers to the ISD and HE MgO layers together. An SRO film (thickness  $\approx 100\text{ nm}$ ) was deposited on the ISD-MgO substrate by pulsed laser deposition (PLD) at  $770^\circ\text{C}$  and an oxygen pressure of 50 mTorr. YBCO was

then deposited on the SRO-buffered ISD MgO substrate at 760°C and 180 mTorr oxygen pressure. YBCO films, 300 nm or 450 nm thick, were made. After deposition of the YBCO layer, it was annealed at 450°C for 90 min at an oxygen pressure of 750 Torr. Further details of the ISD process are given in Ref. 3.

Figure 2 shows an X-ray diffraction (XRD) pattern of YBCO on an SRO-buffered ISD MgO substrate. The peaks that correspond to (00 $l$ ) Miller indices ( $l = 1,2,3,4,5,6$ ) are very strong, showing that the film was highly textured, with a strong  $c$ -axis orientation. An  $\omega$ -scan of the YBCO (005) peak gave a full width at half-maximum (FWHM) of 3.76°, showing good out-of-plane texture.  $\phi$ -scans of the SRO (020) and MgO (200) reflections (Fig. 3) gave FWHM's of 7.38° for SRO (020), and  $\approx$ 10° for MgO (200); a  $\phi$ -scan of the YBCO (103) peak (Fig. 4) had a FWHM of 8.69°, indicating good in-plane texture. The YBCO (103) FWHM has been as low as 6.4° for other films.

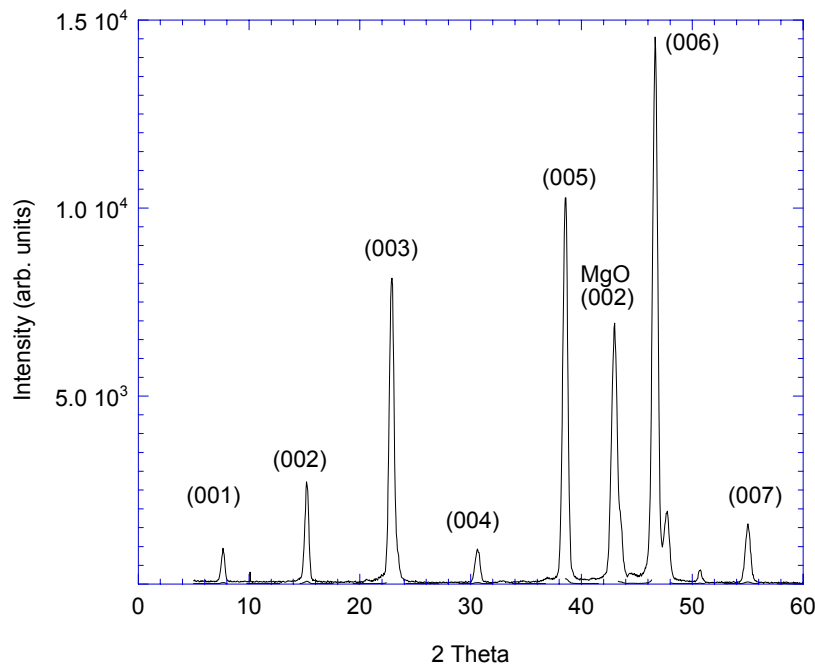


Fig. 2. X-ray diffraction pattern of YBCO/SRO/ISD MgO/HC structure.

The  $T_c$  of 0.3- $\mu$ m-thick YBCO on SRO-buffered ISD MgO was measured by an inductive method; its  $J_c$  was measured by the four-probe method against a 1- $\mu$ V/cm criterion. Figure 5 shows that the  $J_c$  of the YBCO was 280 kA/cm<sup>2</sup> at 77 K and zero applied magnetic field. We previously reported [2]  $J_c$ 's of 30-100 kA/cm<sup>2</sup> for thicker (1.4  $\mu$ m) YBCO films on SRO-buffered ISD MgO. Although the latest result indicates some improvement in transport properties, Fig. 6 shows that the film exhibited a relatively low  $T_c$  (onset) of  $\approx$ 87 K, indicating that the YBCO deposition conditions need

further refinement. This conclusion is consistent with scanning electron microscopy/energy dispersive spectroscopy (SEM/EDS) results that show the composition of the YBCO film is not completely homogeneous.

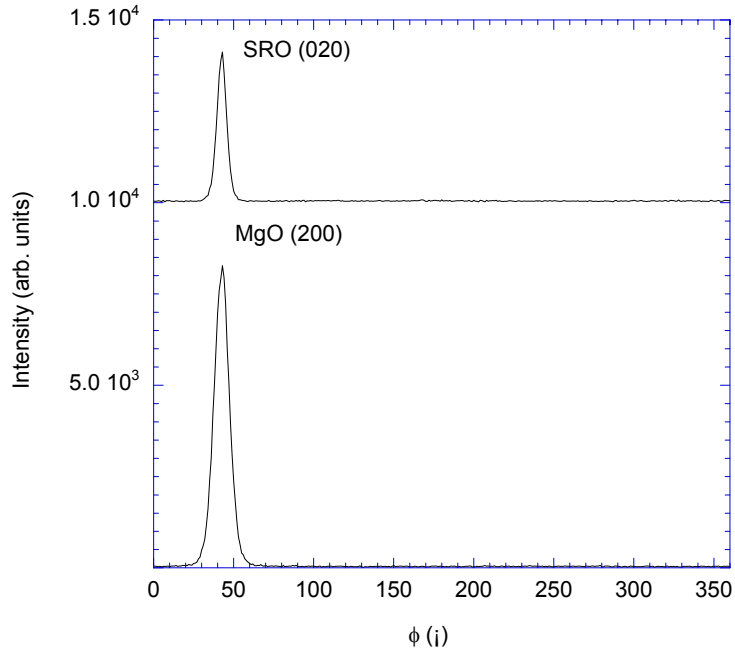


Fig. 3. SRO (020) and MgO (200)  $\phi$ -scans for YBCO/SRO/ISD MgO/HC structure.

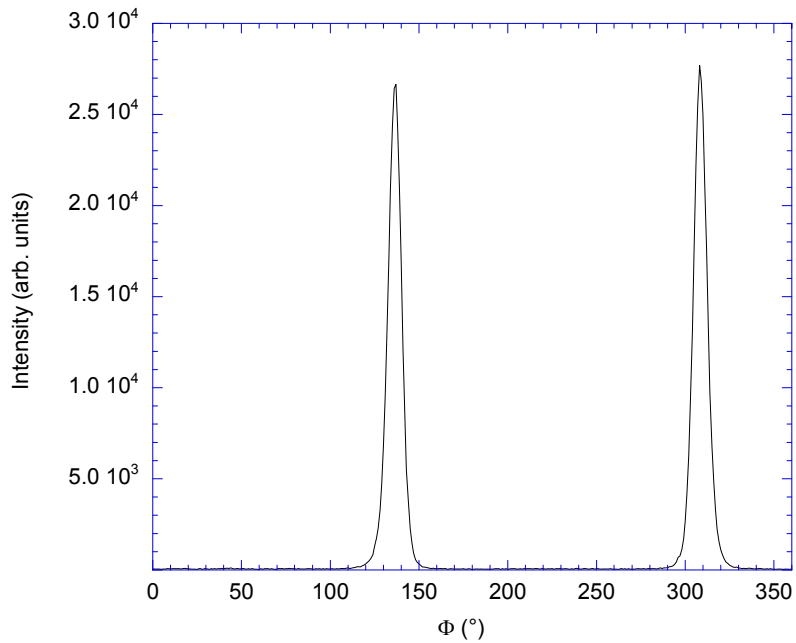


Fig. 4. YBCO (103)  $\phi$ -scan for YBCO/SRO/ISD MgO/HC structure.

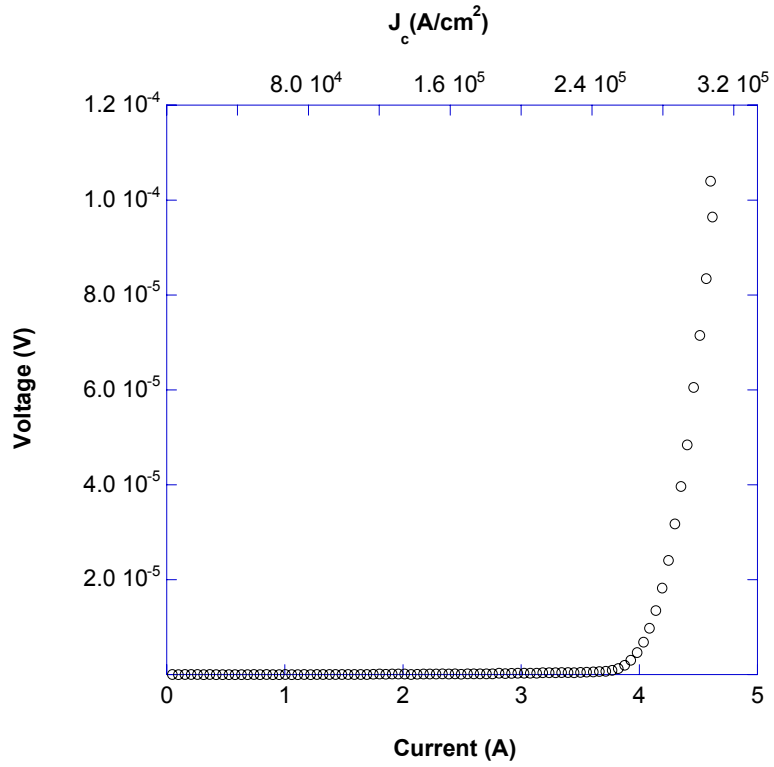


Fig. 5. Transport critical current density ( $J_c$ ) of YBCO/SRO/ISD MgO/HC structure.

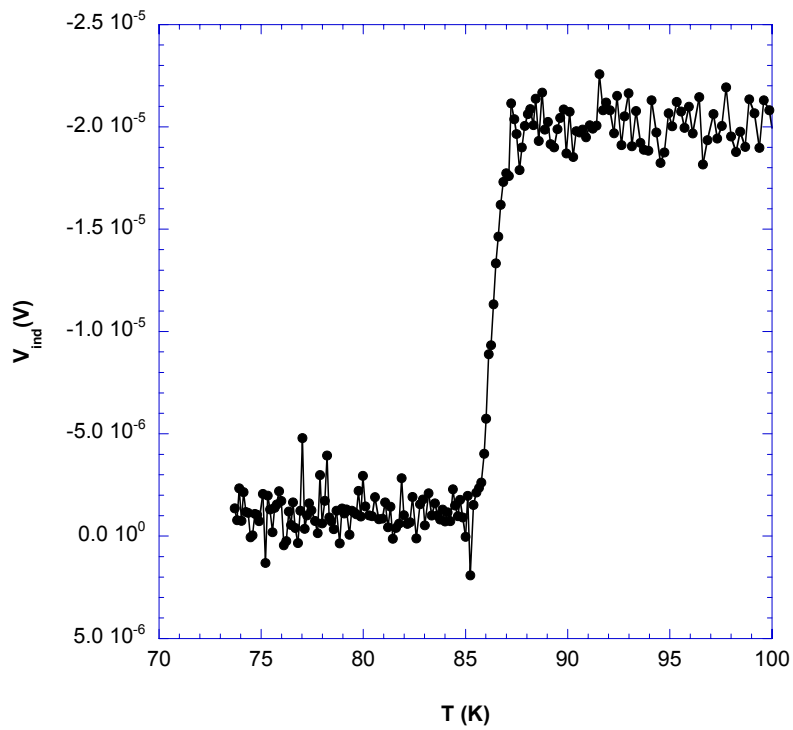


Fig. 6. Critical temperature ( $T_c$ ) of YBCO/SRO/ISD MgO/HC structure.

## Basic Features of Raman Microscopy Relevant to Examination of Coated Conductors

Raman spectroscopy continues to serve as a powerful, comprehensive characterization tool for examining  $\text{MBCa}_2\text{Cu}_3\text{O}_{7-\delta}$  (MBCO). In this report we begin with a rudimentary discussion of the Raman active phonon properties of the MBCO crystal structure for  $x = 0$  (orthorhombic MBCO) and  $x = 1$  (tetragonal MBCO). We couple that discussion with a description of how the observational features of these phonons are influenced by the epitaxial (single-crystal-like) nature of MBCO films on textured substrates. We then describe the results of a detailed Raman microprobe study of a 1.25-m-long YBCO coated conductor specimen produced by Dominic Lee at ORNL.

From factor group analysis one determines that both the orthorhombic and tetragonal MBCO structures (referred to herein as MBCO/O and MBCO/T, respectively) have fifteen Raman active vibrational degrees of freedom [4]. For MBCO/O, the motional vector of five of these phonons is along the **c**-axis direction, whereas the motional vector for the other ten phonons is in the **a,b** planes. For MBCO/T, there are, again, five nondegenerate phonons, with motional vectors along the **c**-axis and five doubly degenerate phonons with motional vectors in the **a,b** planes. The only phonons regularly detected for MBCO are the ones with motional vectors along the **c**-axis. One speculation about why this is so is based on the notion that MBCO exhibits characteristics of a ceramic-like material in the **c**-axis direction, and those of a pseudometal in the **a,b** planes. Because metals are notoriously poor Raman scatterers when a visible wavelength excitation source (invariably a laser) is used to excite the Raman scattering, it is not surprising that the **a,b**-plane phonons (mostly involving vibrations in the copper-oxygen planes of MBCO) fail to appear in visible-wavelength-excited Raman spectra.

The motional vectors for the five **c**-axis phonons of the MBCO structure, which turn out to be identical for both MBCO/O and MBCO/T, are shown in Fig. 7, together with typical values for the phonon frequencies of the two MBCO crystal types. Each of these phonons has its own unique set of polarizability tensor elements, and these sets produce various scattering intensities, depending on the orientation of the MBCO crystal with respect to the direction of propagation of the incident laser ( $\lambda$ ) and the direction of observation (**I**) of the Raman scattering [5]. Typically, when a Raman microprobe is used to examine an MBCO coated conductor specimen, the excitation/detection configuration is such that the introduction of the laser and the observation of Raman scattering are both performed perpendicular to the plane of the substrate (i.e., by employing a common optical element) and, hence, parallel to the **c**-axis of the MBCO film. The observed intensities of the MBCO/O and MBCO/T phonons for this case are illustrated in Fig. 8 by the two spectra marked with the designation  $\lambda // \text{c} \ \& \ \text{I} // \text{c}$ . These spectra were obtained by using oriented bulk specimens of YBCO/O and YBCO/T produced by zone-melting methods. A strikingly

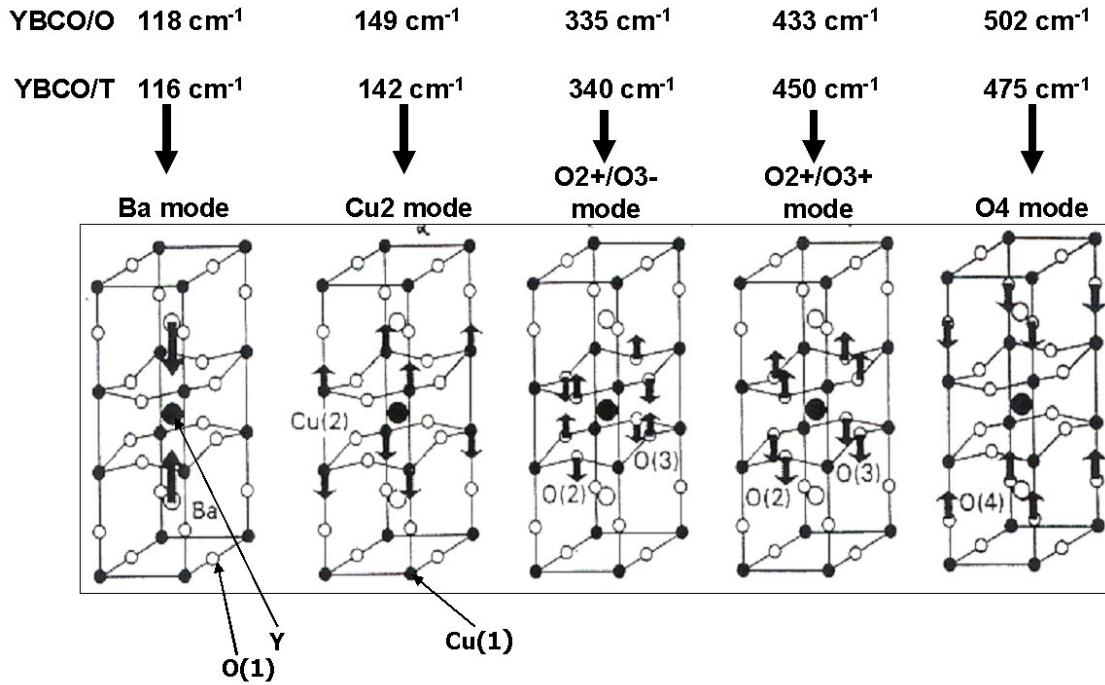


Fig. 7. Atom motion vectors for the five Raman-active *c*-axis phonons of orthorhombic and tetragonal MBCO (MBCO/O and MBCO/T, respectively), together with typical frequency values for each MBCO crystal type.

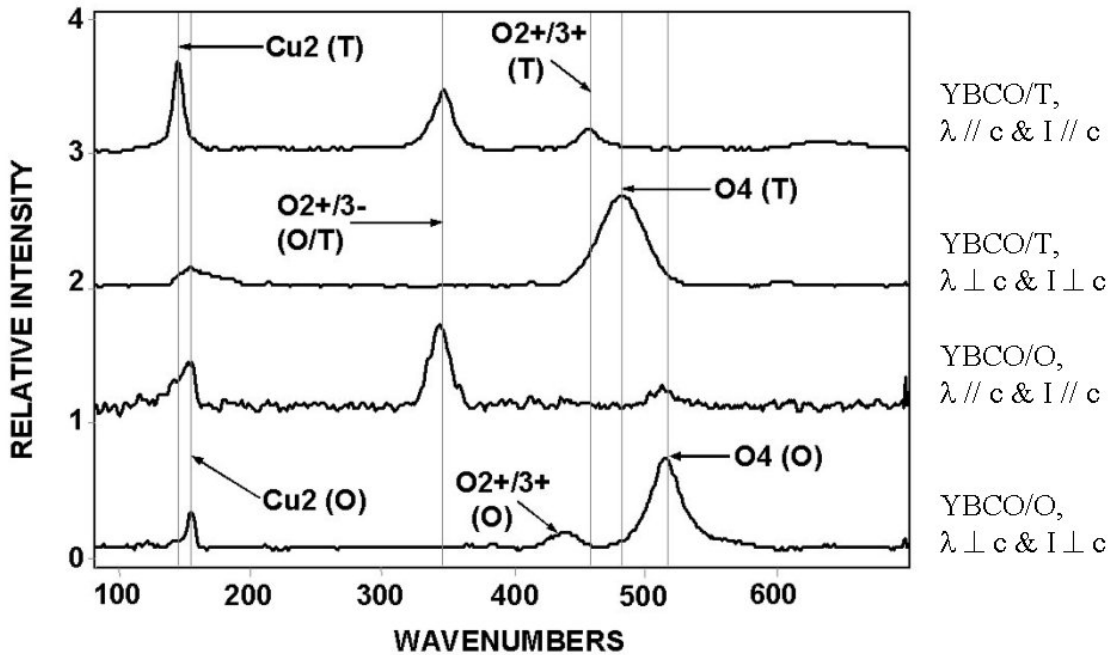


Fig. 8. Raman spectra of bulk, textured (melt-processed) samples of MBCO/O and MBCO/T for two orientations of incident excitation laser ( $\lambda$ ) and observation direction ( $I$ ).

different phonon intensity pattern is obtained when both  $\lambda$  and  $I$  are perpendicular to the  $c$ -axis. In Fig. 8, we also show the corresponding spectra for this case (designated as  $\lambda \perp c$  &  $I \perp c$ ) because it comes into play when the MBCO grains tip out of the plane of the substrate and/or when “a-axis” grain growth occurs. Note in Fig. 8 that, for perfectly epitaxial MBCO/O in the  $\lambda // c$  &  $I // c$  configuration, one should observe the O2+/O3- and Cu2 modes but not the O4 mode. Conversely, in the  $\lambda \perp c$  &  $I \perp c$  configuration, one should observe the O4 and Cu2 modes but not the O2+/O3- mode. In the case of a specimen composed of a mixture of epitaxial, tilted, and/or a-axis MBCO/O grains, one is likely to observe Raman spectra that are a mix of the ones shown in Fig. 8. Furthermore, if MBCO/T is present alone or in combination with MBCO/O, one is likely to observe a spectrum composed of a mix of two or more of the four spectra shown in Fig. 8.

Using the results in Fig. 8 as a basis, we can determine many important characteristics of MBCO coated conductor films from their Raman spectra. For example, we can gauge the relative amounts of epitaxial versus tilted/a-axis grains from the relative intensities of the O2+/O3- and O4 modes, distinguish MBCO/O from MBCO/T by using the frequencies of the O4, Cu2, and O2+/O3+ phonons, and estimate the extent of oxygenation of MBCO (i.e., the value of  $x$ ) from the frequency of the O4 mode. Coupling this capability with our previously reported success in detecting many of the relevant secondary nonsuperconducting phases that occur during precursor heat treatment to form MBCO films (e.g., CuO, BaF<sub>2</sub>, BaCeO<sub>3</sub>, and barium cuprates), it becomes demonstrably clear that Raman microscopy is a globally useful methodology for interrogating MBCO coated conductors. Furthermore, to make the technique applicable to long-length conductors, we have constructed a reel-to-reel attachment for our existing Raman microprobe (see Fig. 9) that allows us to examine tapes up to 12 m long. In the next section, we describe the application of this methodology to specific meter-length coated conductor specimens.

### Raman Microscopy Examination of Time-Gradient-Treated Coated Conductors

Reel-to-reel (R2R) Raman microscopy is now being performed routinely in our laboratory. Although the technique is providing substantive information when employed to examine fully processed tapes, we have also found that it is especially useful for characterizing phase evolution in tapes that have been processed to obtain a gradation of transformed precursor states. Specifically, Dominic Lee at ORNL has developed a method for creating such tapes. The method consists of reeling a precursor-coated substrate into/through a preheated furnace at a controlled rate such that each increment of the precursor spends a different amount of time at the selected precursor transformation temperature. The tape feed rate is chosen such that the leading edge of the precursor is overprocessed, the trailing edge is essentially unprocessed, and an entire spectrum of phase conversion states exists in between.

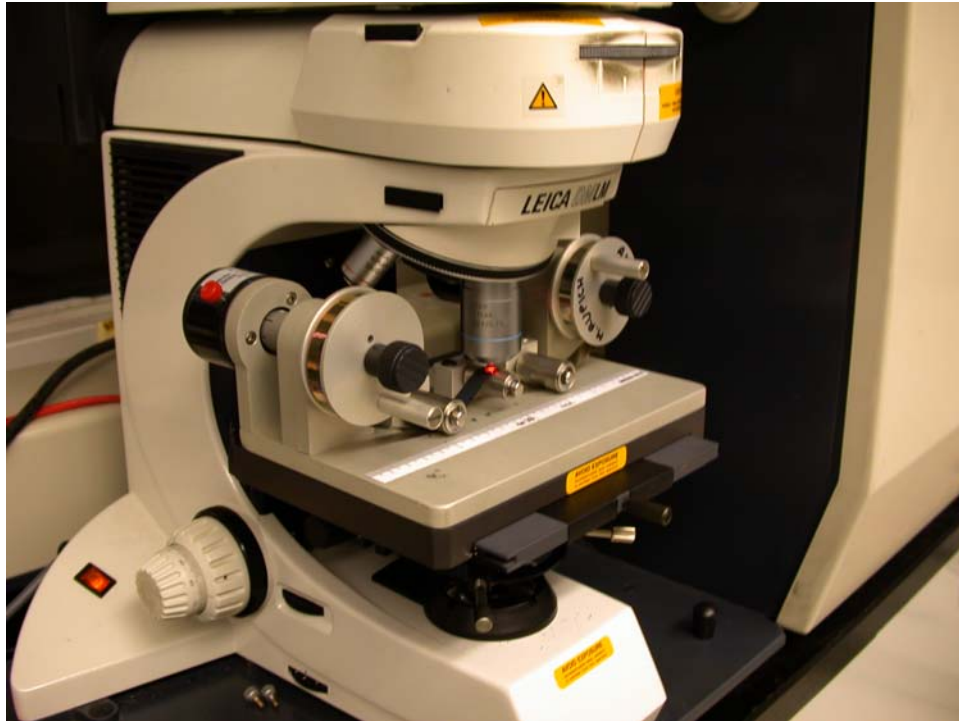


*Fig. 9. Picture of reel-to-reel (R2R) device used to feed and control long-length coated conductor tape specimens during Raman microscopy examinations. R2R device is shown in position on microscope stage of Raman microprobe.*

When the leading edge of the coated section reaches the end of the hot zone, the tape is rapidly reeled back out of the furnace to quench the existing phase states. During the past year, we have examined two of these time-gradient-processed tapes produced by Dominic Lee. Both were YBCO/CeO<sub>2</sub> (150 nm)/YSZ(200 nm)/Y<sub>2</sub>O<sub>3</sub>(15 nm)/Ni (1 μm)/Ni-W(50 μm) embodiments that consisted of ≈1.25 meters of electron-beam-deposited Y-BaF<sub>2</sub>-Cu precursor (with sufficient leader tape attached to each end to allow reeling). The specimens were coated to produce two thicknesses of YBCO, 280 nm in one case and 1000 nm in the second case. Inasmuch as the results obtained by Raman microscopy examination of these two tapes were the same in nearly all respects, we will limit the discussion in this report to the findings for the 280 nm YBCO tape.

A sketch of the time/temperature/distance relationship for the 280-nm YBCO tape is shown in Fig. 10. The precursor transformation temperature used for this sample was 740°C. The consecutive increments of the precursor spent times ranging from “zero” to 150 min at this temperature. In addition, there were increments of precursor near the trailing end of the coated section (the ramp section) that experienced peak temperatures ranging from 600 to 740°C before the quench. In the Raman microscopy examination of this tape, we used a partially defocused excitation laser (633 nm wavelength) to probe two spots (≈6 μm in diam.) at each distance along the tape. The two spots were chosen to be one quarter of the way in from the top edge (as depicted in Fig. 10) and three

quarters of the way in, respectively. This was done to look for evidence of transverse variations in the phase composition along the length of the precursor coating. However, because a discernable difference in the two spectra was seen in very few instances, this report will focus on the end-to-end variations by using the averaged value of the two Raman spectra recorded at each probed lengthwise location. The following paragraphs present a segment-by-segment synopsis that starts at the trailing end of the precursor zone, highlights the key findings and implications of the Raman results, and points out the instances where these results reinforce and transcend the findings of an R2R XRD analysis of the same tape performed at ORNL.

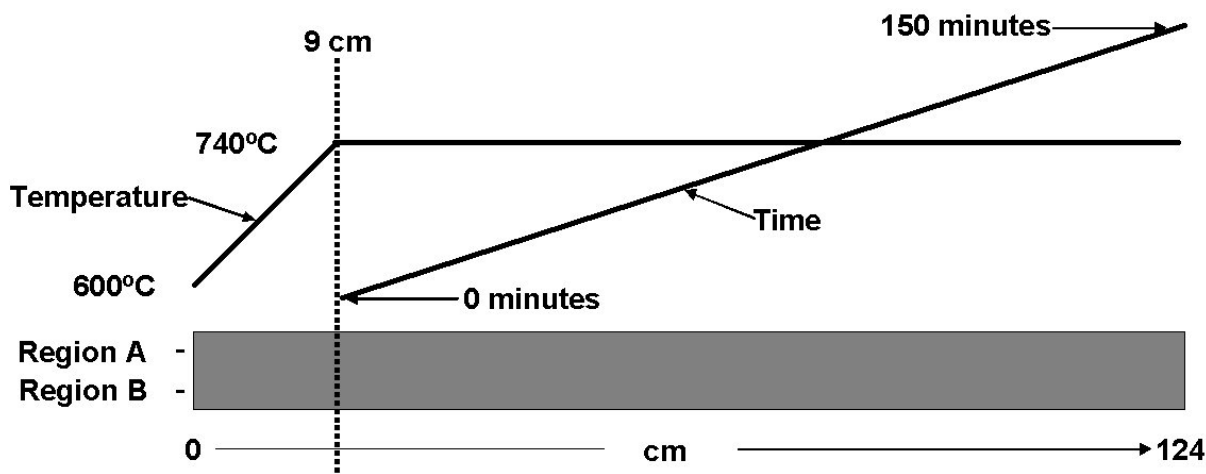


Fig. 10. Schematic diagram illustrating time and temperature profiles used by D. Lee at ORNL to produce time-gradient-processed 280-nm-thick YBCO film on 1.25 m metal substrate.

The Ramp Zone (650 to 740°C) The Raman spectra of increments of the precursor in this zone (see Fig. 11) exhibit two broad diffuse band envelopes, one between 100 and 200  $\text{cm}^{-1}$  and another between 500 and 700  $\text{cm}^{-1}$ , indicating the dominant presence of an amorphous mush from which  $\text{CuO}$  ( $\approx 300 \text{ cm}^{-1}$ ) appears as the first crystalline phase.  $\text{BaF}_2$ , the cubic form of which exhibits a characteristic phonon at 242  $\text{cm}^{-1}$ , is not detected in this region (3 to 8 cm) by Raman microscopy, and the ORNL XRD results likewise show little evidence of cubic  $\text{BaF}_2$  in this region. By the time the precursor has reached 740°C, the  $\text{CuO}$  phonon dominates the spectrum, but other sharp modes begin to appear as shown in Fig. 12, where we present a comparison of the 3-cm increment (650°C maximum temperature) and the 9-cm increment (initial minute at 740°C) to provide a beginning-to-end perspective of the aggregate phase transformation that takes place in the ramp segment.

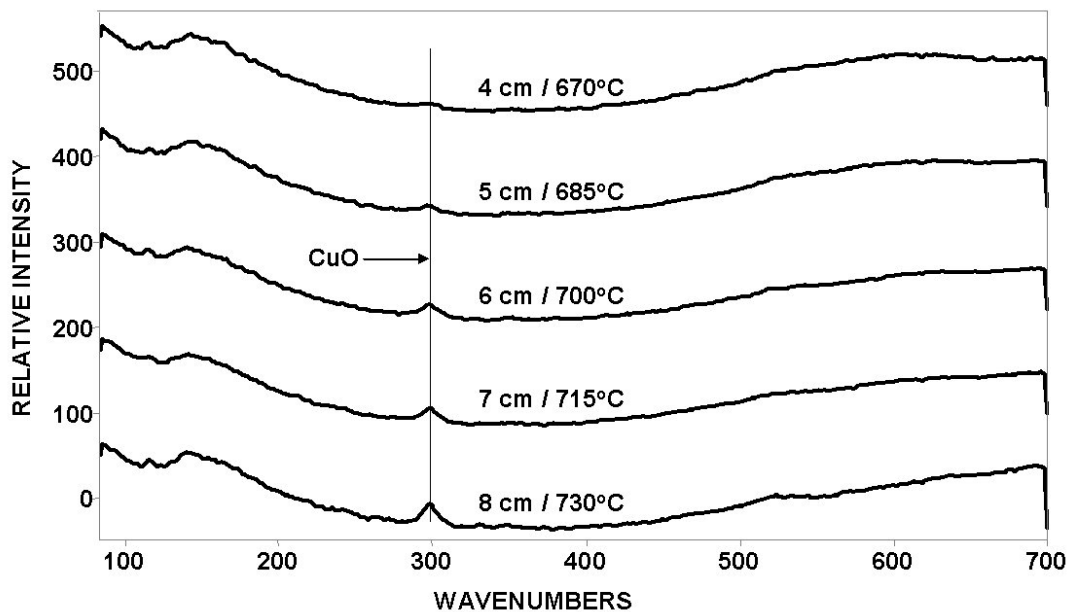


Fig. 11. Raman spectra of Y-BaF<sub>2</sub>-Cu precursor at five increments in ramp zone of 1.25-m time-gradient-processed tape received from ORNL. Indicated temperature is maximum reached before quench at that location.

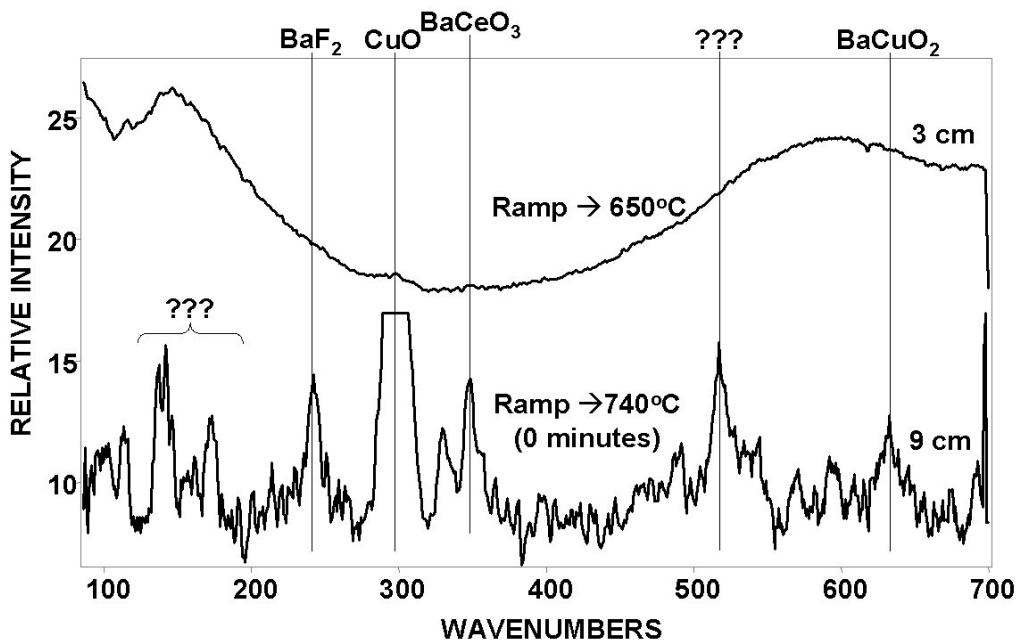


Fig. 12. Raman spectra recorded at 650°C ramp increment and at increment where precursor just reached transformation temperature (740°C) before quench. Note onset of crystallization in latter case (lower spectrum).

Overview of Phase Evolution on the 740°C Plateau Figure 13 presents an overview of phase transformation along the 740°C plateau. On the right-hand side of this figure, we correlate each spectrum with the elapsed time at 740°C to provide a global view of the overall reaction kinetics. In just a few minutes at 740°C, the broad bands associated with the amorphous mush are completely gone, and several new crystalline phases (in addition to CuO) are clearly evident. In just a little over ten min, phonons attributable to BaF<sub>2</sub> and BaCeO<sub>3</sub> are apparent, YBCO is starting to form, and other bands are present in the spectra, which we will subsequently discuss and assign. In a little over 30 min the spectra are dominated by YBCO/T phonons; in fact, the last vestiges of CuO appear at the 34-min point. It is noteworthy that the ORNL XRD scans of this region detected the in-growth of BaF<sub>2</sub> and BaCeO<sub>3</sub> and the formation of YBCO (not specifically the “T” form) but not the CuO or other new phases.

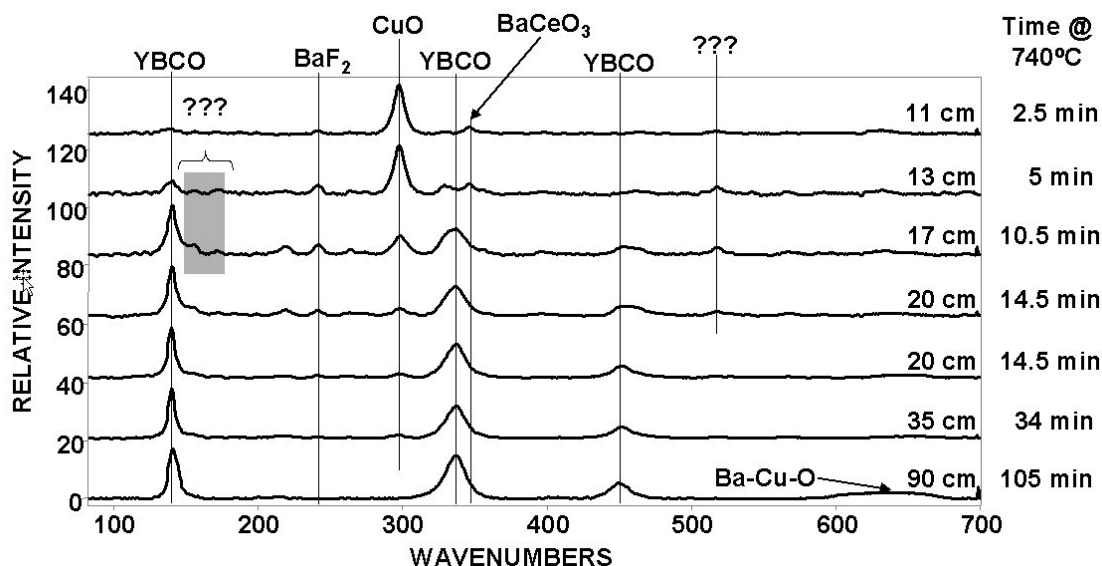


Fig. 13. Raman spectra of increments along portion of 1.25-m time-gradient-processed YBCO tape that reached treatment temperature of 740°C. Time each increment spent at 740°C before quench is indicated along right side of plot.

New Phases in the First 20 Min at 740°C A series of bands that begins to emerge in the first few minutes at 740°C and persists through the first 20 min exhibits a compelling correlation with the phonon pattern of the Y<sub>2</sub>Cu<sub>2</sub>O<sub>5</sub> phase (referred to hereinafter as 202). This correlation can be seen in Fig. 14, where we plot the precursor spectra for ≈0 and ≈16 min of treatment at 740°C, together with the spectrum of pure 202 powder, which was recorded under the same instrument conditions used to examine the 1.25-m tape. The correlation at 0 min is clearer than that at 16 min, where YBCO and BaF<sub>2</sub> modes tend to mask some of the 202 modes. In addition, modes in the range of 590 to 650 cm<sup>-1</sup> are attributed to barium cuprates (Ba-Cu-O) [4]. These results

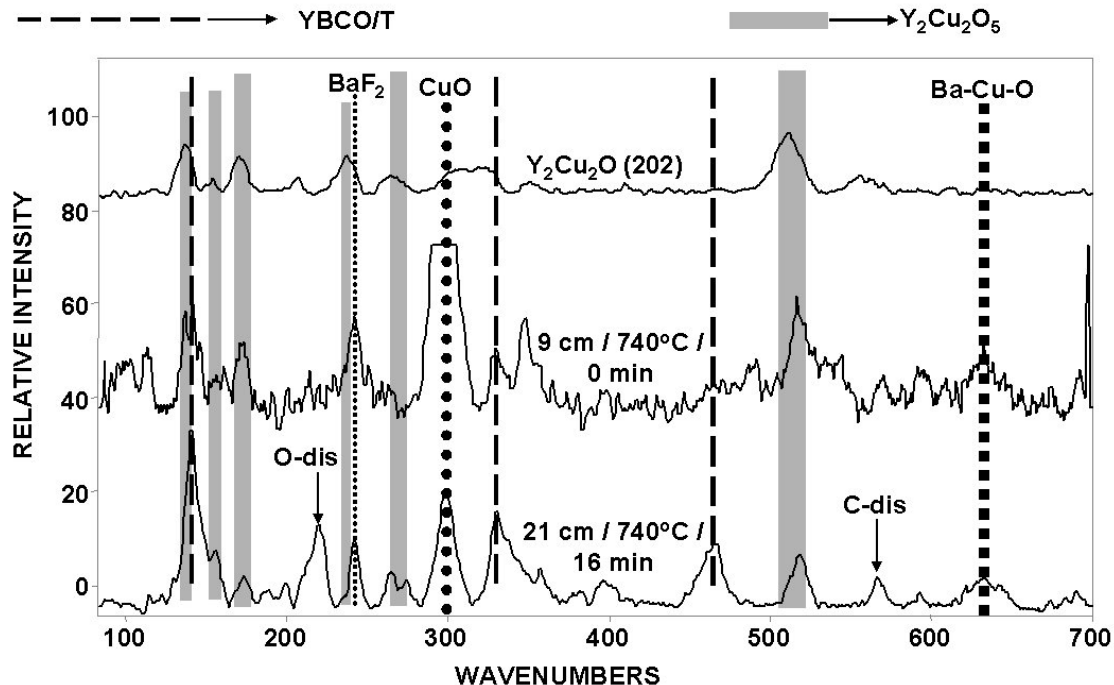


Fig. 14. Plot showing correlation of Raman bands for pure  $Y_2Cu_2O_5$  powder specimen (top spectrum) with bands seen in early stages of YBCO precursor transformation during time-gradient-processing of 1.25-m YBCO tape specimen. Middle spectrum is for 9-cm increment, which just reached  $740^\circ C$  before quench; lower spectrum is for 16-cm increment, which spent  $\approx 16$  min at  $740^\circ C$  before quench. "O-dis" and "C-dis" are bands attributed to oxygen-disorder- and cation-disorder-induced phonons of YBCO [6].

imply that the 202 and Ba-Cu-O phases (along with CuO) are intermediates to YBCO formation. Furthermore, none of these phases was conclusively identified during the ORNL XRD examinations. Figure 15 is included to show that these phases persist through the early stages of YBCO formation.

The Heartland of YBCO Formation and the "Sweet Spot" Figure 16 presents Raman spectra that cover the time range at  $740^\circ C$ , extending from the final appearance of modes due to intermediates (i.e., CuO, 202, and Ba-Cu-O), through the region of optimum YBCO/T presence, to the onset of an overprocessed state, where Ba-Cu-O modes reappear. We believe these results define a "sweet spot" in the time-at- $740^\circ C$  progression where the film is composed of nearly phase-pure YBCO/T. This "sweet spot" occurs in the range from 50 to 70 min at  $740^\circ C$ . In the blowup of the 40-79-min region, shown in Fig. 17, we see little evidence of any phonons other than the three characteristic ones due to YBCO/T but do note the onset of the well-studied YBCO cation disorder mode ( $\approx 580$   $cm^{-1}$  [6]) in the 79-min spectrum. The "sweet spot"

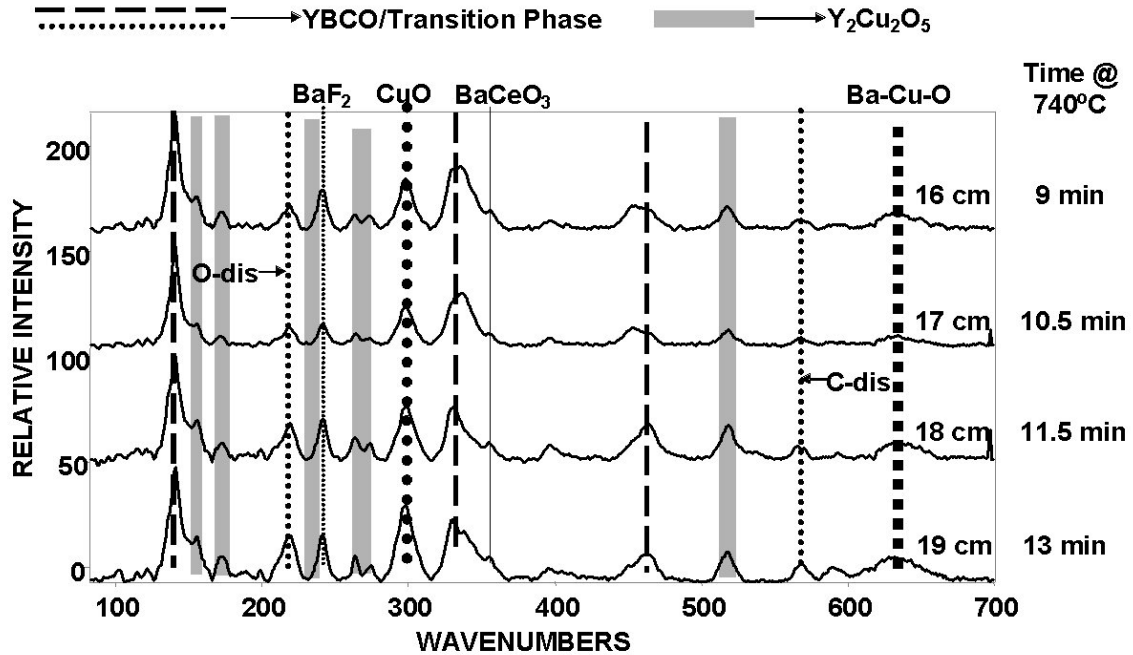


Fig. 15. Raman spectra of increments in midportion of phase transition region, showing persistence of  $Y_2Cu_2O_5$  and CuO phonons in early stages of YBCO formation along 1.25-m YBCO time-gradient-processed tape.

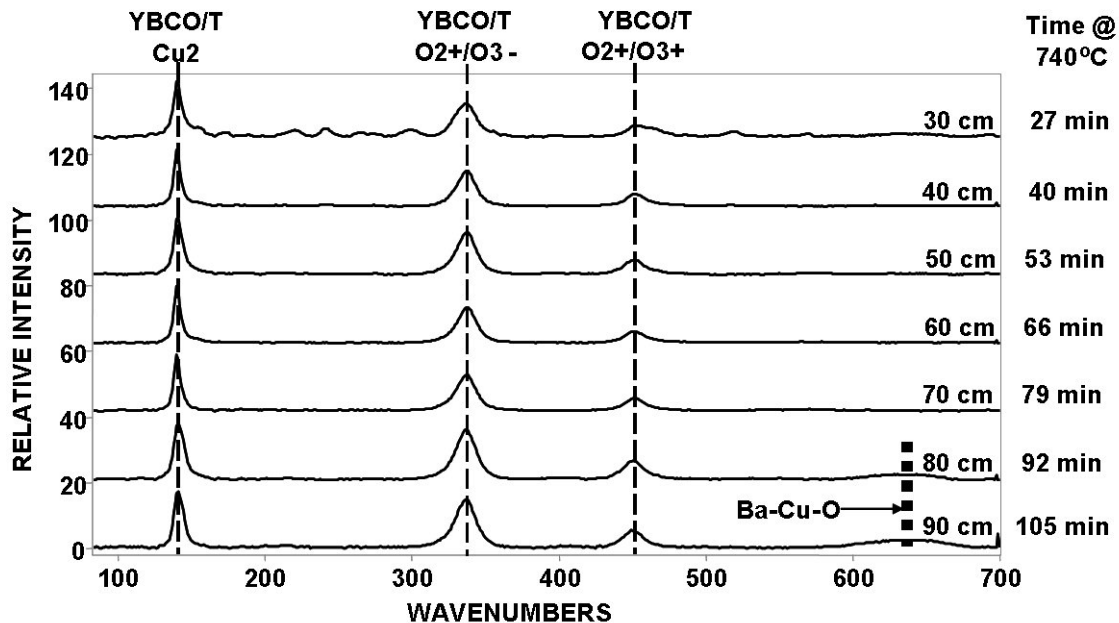


Fig. 16. Raman spectra of increments that range from end of transformation region to beginning of over-processed region along 1.25-m YBCO time-gradient-processed tape. "Sweet spot" appears to occur in range of 50-70 min at 740°C for 280-nm-thick YBCO film.

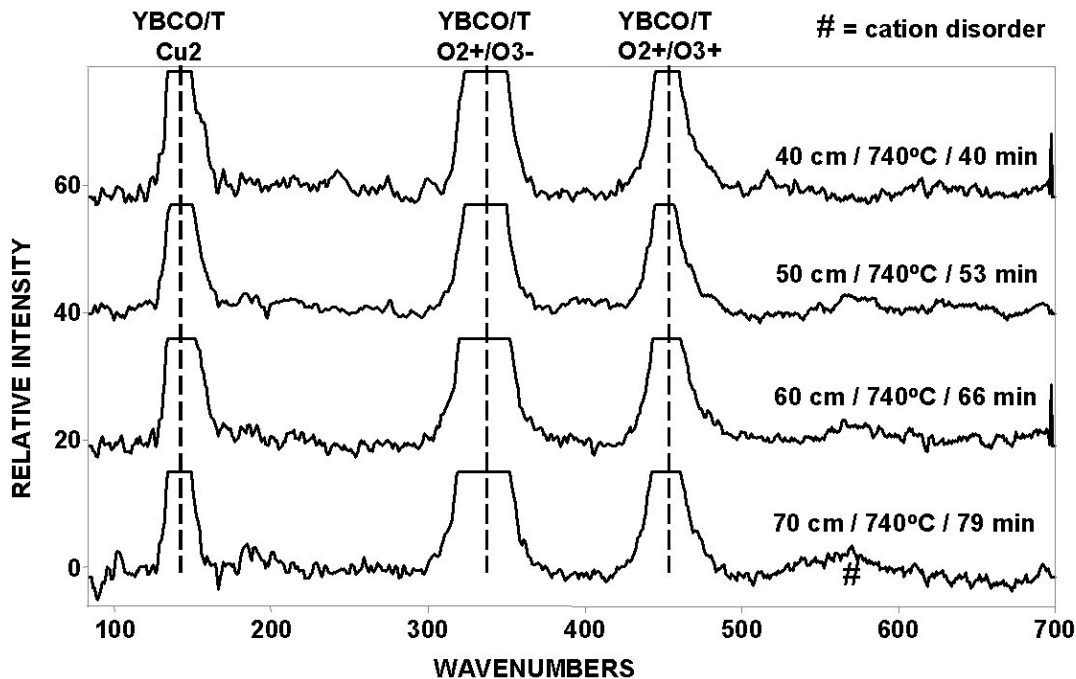


Fig. 17. Intensity-scale-expanded Raman spectra at four increments in region of "sweet spot" along 1.25-m YBCO time-gradient-processed tape. No discernable evidence of residual second phases and only minimal evidence of cation disorder can be observed.

observed for the 1000-nm YBCO tape specimen produced by Dominic Lee corresponds to  $\approx 220$ -230 min at 740°C (roughly four times that for the 280-nm YBCO tape specimen), illustrating the same approximately linear relationship between processing time and YBCO film thickness that was deduced from the ORNL XRD measurements.

We are presently engaged in a detailed assessment of a plausible reaction mechanism for YBCO/T formation from the Y-BaF<sub>2</sub>-Cu precursor. The mechanism we are investigating consists of a series of binary reactions that involves the phases we detected by Raman microscopy (CuO, 202, Ba-Cu-O, and, of course, YBCO/T), the H<sub>2</sub>O that is present in the process gas stream employed during the 740°C soak, and the herein-proposed intermediate phase Ba(OH)F. Ample evidence for the existence of Ba(OH)F is coming from literature searches that cover the thermodynamic and spectroscopic properties of alkaline earth hydroxy halides [7]. We will describe the results of this assessment in the next Quarterly Progress Report.

#### Evaluation of Strain Tolerance in YBCO Coated Conductors

Coated conductors will encounter mechanical strains/stresses both during processing and in service. These strains/stresses may cause microcracking and damage to the superconductor layer, possibly degrading its superconducting properties and reducing its service life. Therefore, it is important to evaluate the critical value of strain

(strain tolerance) at which conductors exhibit degradation in superconductivity, and subsequently, develop an understanding of the relationship between strain tolerance and various processing parameters. Our initial focus in this area was on evaluating the effect of the YBCO thickness on the tensile bend-strain tolerance of multilayer coated conductors. Specifically, coated conductors were fabricated with the architecture HC/ISD MgO/HE MgO/YSZ/CeO<sub>2</sub>/YBCO. For this study, the thickness of the HC substrate, ISD and HE MgO layers, and the YSZ and CeO<sub>2</sub> buffer layers were kept constant, and the thickness of the YBCO layer was varied from 0.1 to 0.5 μm. The ISD MgO layer was 1 μm thick and was deposited at room temperature by the electron beam evaporation technique at a deposition angle of 55°. The HE MgO layer (0.5 μm thick) was deposited at 700°C with the same ISD system, at a deposition angle of 0°. The YSZ (thickness ≈0.1-0.2 μm) and CeO<sub>2</sub> (thickness ≈10 nm) layers were deposited at 800°C by pulsed laser deposition (PLD). The top YBCO layer was deposited at 760°C by the PLD method.

Strain tolerance of the ISD coated conductors was measured by first subjecting the conductor to increasing levels of tensile bend strain ( $\epsilon$ ), followed by measuring critical current ( $I_c$ ) by the inductive method. The critical current ( $I_c$ ) of the strained conductors, normalized with respect to the critical current ( $I_{c0}$ ) in the unstrained condition, has been plotted as a function of applied bend strain ( $\epsilon$ ) in Fig. 18. For a given YBCO layer

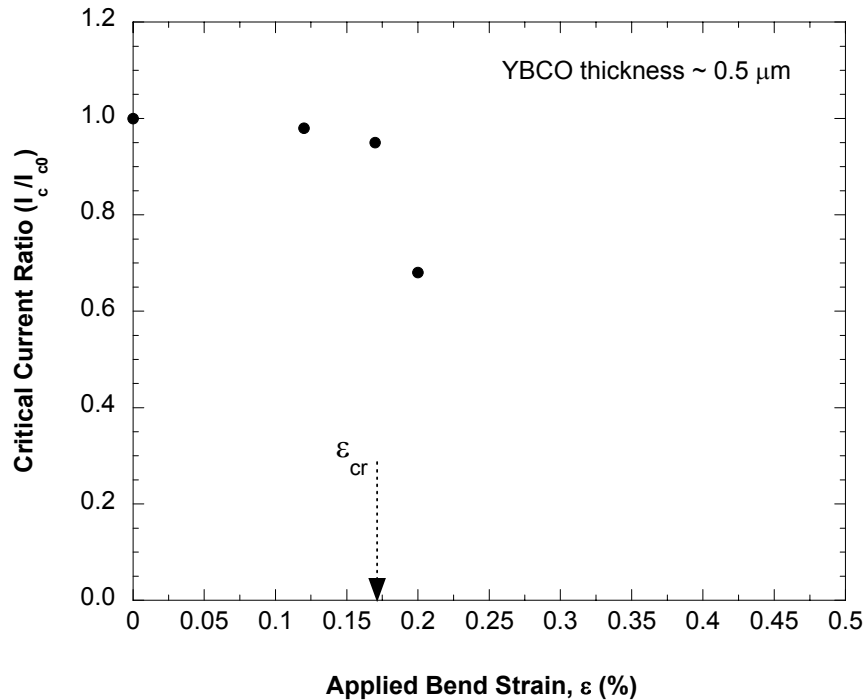


Fig. 18. Variation of critical current ratio ( $I_c/I_{c0}$ ) as a function of applied bend strain  $\epsilon$ . The critical strain  $\epsilon_{cr} = 0.17\%$ .

thickness, the critical strain ( $\epsilon_{cr}$ ) was taken as the strain at which the conductor exhibited the onset of degradation in  $I_c$ . A variation of  $\epsilon_{cr}$  with YBCO layer thickness is shown in Fig. 19. Also, plotted in the figure are critical strain values that were calculated analytically by using an assumed toughness of  $0.4 \text{ MPa}\sqrt{\text{m}}$  for the YBCO. As seen in the figure, the measured  $\epsilon_{cr}$  decreased from 0.39% for YBCO with a thickness of  $0.2 \mu\text{m}$  to 0.17% for YBCO with a thickness of  $0.5 \mu\text{m}$ . This inverse relationship between  $\epsilon_{cr}$  and YBCO layer thickness is consistent with the analytical prediction.

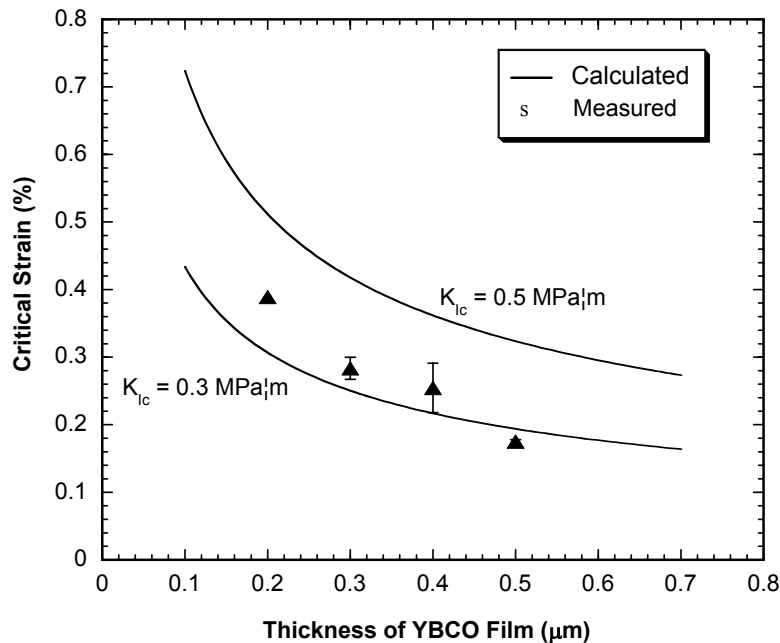


Fig. 19. Dependence of measured critical strain  $\epsilon_{cr}$  on YBCO layer thickness. Calculated values of critical strain based on analytical prediction are also shown.

## References

- [1]. Argonne National Laboratory Practical Superconductor Development for Electrical Power Application, Quarterly Report for Jul.-Sept., 2002.
- [2]. Argonne National Laboratory Practical Superconductor Development for Electrical Power Application, Quarterly Report for Jan.-Mar., 2003.
- [3]. B. Ma, M. Li, Y. A. Jee, B. L. Fisher, and U. Balachandran, "Inclined Substrate Deposition of Biaxially Textured Magnesium Oxide Films for YBCO Coated Conductors," *Physica C*, **366**, 270-276 (2002).
- [4]. J. R. Ferraro and V. A. Maroni, *Applied Spectroscopy* **44**, 351-366 (1990)
- [5]. M. N. Iliev, *American Chemical Society Symposium Series* **730**, 107-119 (1999).

[6]. G. Gibson, L. F. Cohen, R. G. Humphreys, and J. L. MacManus-Driscoll, *Physica C* **333**, 139-145 (2000).

[7]. S. Peter, F. Altorfer, W. Bührer, and H. D. Lutz, *Journal of Solid State Chemistry* **151**, 267-271 (2000).

## **Interactions**

Vic Maroni attended a Wire Development Group meeting on April 9-10, 2003 at the University of Wisconsin/Madison. AMSC, LANL, UWM, and ANL participated.

Y. S. Cha attended the Technical Advisory Board meeting and the Design Review meeting for the Matrix fault current limiter proposed by SuperPower (June 10-12, 2003) at SuperPower in Schenectady, NY.

Balu Balachandran presented ANL's research plans and accomplishments at the FWP Review in Washington DC on April 14, 2003.

Dean Miller, Beihai Ma, Roxanne Baurceanu and Shankar Srinivasan attended the American Ceramic Society meeting in Nashville, TN, April 27-30, 2003 and presented papers.

Balu Balachandran attended the ANL-SuperPower MOCVD CRADA project review in Albany, NY on May 7, 2003.

Balu Balachandran attended the DOE coated conductor program review at SuperPower in Albany, NY on May 8, 2003.

Balu Balachandran participated by phone the CCAS meeting held in New York on June 18, 2003.

## **Publications and Presentations**

### Published/Presented

V. K. Vlasko-Vlasov, H. Claus, U. Welp, K. E. Gray (MSD), B. Ma, and U. Balachandran, Improving Ratio of the Grain Boundary and Bulk Critical Currents in  $\text{YBa}_2\text{Cu}_3\text{O}_{7-\delta}$  Films, Submitted to Appl. Phys. Lett. (June 2003).

M. Li, B. Ma, R. E. Koritala, B. L. Fisher, K. Venkataraman, V. A. Maroni, V. Vlasko-Vlasov, P. Berghuis, U. Welp, K. E. Gray, and U. Balachandran, Pulsed Laser Deposition

of c-Axis Untilted YBCO Films on c-Axis Tilted ISD MgO-Buffered Metallic Substrates, *Physica C* **387** (2003) 373-381.

Y. S. Cha, An Empirical Correlation for  $E(J,T)$  of a Melt-Cast-Processed BSCCO-2212 Superconductor Under Self Field, *IEEE Transactions on Applied Superconductivity*, Vol. 13, No. 2, June 2003, pp. 2028-2031.

S. Hanany, T. Matsumura, B. Johnson, T. Jones (U. of Minnesota); J. R. Hull; and Ki B. Ma (Texas Ctr. for Superconductivity), A Cosmic Microwave Background Radiation Polarimeter Using Superconducting Bearings, *IEEE Transactions on Applied Superconductivity*, Vol. 13, No. 2, June 2003, pp. 2128-2133.

R. E. Koritala, D. J. Miller, B. Ma, M. Li, B. L. Fisher, and U. Balachandran, Texture Development of MgO Buffer Layers Grown by Inclined Substrate Deposition, *IEEE Transactions on Applied Superconductivity*, Vol. 13, No. 2, June 2003, pp. 2691-2694.

B. Ma, M. Li, R. E. Koritala, B. L. Fisher, R. A. Erck, S. E. Dorris, D. J. Miller, and U. Balachandran, Biaxially Aligned Template Films Fabricated by Inclined-Substrate Deposition for YBCO-Coated Conductor Applications, *IEEE Transactions on Applied Superconductivity*, Vol. 13, No. 2, June 2003, pp. 2695-2698.

T. R. Askew, J. M. Weber (Kalamazoo College); Y. S. Cha, H. Claus, and B. V. Veal, Transient Response of Single-Domain Y-Ba-Cu-O Rings to Pulsed Magnetic Fields, *IEEE Transactions on Applied Superconductivity*, Vol. 13, No. 2, June 2003, pp. 3750-3754.

P. S. Shankar and J. P. Singh, Residual Stress Measurements in YBCO-Coated Conductors, Presented at the 105<sup>th</sup> Ann. Mtg. of the American Ceramic Society, Nashville, April 27-30, 2003.

R. M. Baurceanu, S. E. Dorris, T. Wiencek, B. Ma, V. A. Maroni, K. Venkataraman, and U. Balachandran, Copper Additions to Silver Substrates for  $YBa_2Cu_3O_{7-\delta}$  Coated Conductors, Presented at the 105<sup>th</sup> Ann. Mtg. of the American Ceramic Society, Nashville, April 27-30, 2003.

Y. X. Zhou, M. Mironova, H. Fang (U. of Houston); U. Balachandran; and K. Salama (U. of Houston), New Seeding Method for Texturing Y-Ba-Cu-O Bulk Superconductor: Multiple-Seeded Melt Growth, Presented at the 105<sup>th</sup> Ann. Mtg. of the American Ceramic Society, Nashville, April 27-30, 2003.

U. Balachandran, Practical Superconductor Development for Electric Power Applications, Oral presentation at the FWP Review, Washington, DC, April 14, 2003.

B. Ma, B. L. Fisher, R. E. Koritala, S. E. Dorris, and U. Balachandran, Fabrication of YBCO-Coated Conductors by Inclined-Substrate Deposition, Invited abstract presented at the 105<sup>th</sup> Ann. Mtg. of the American Ceramic Society, Nashville, April 27-30, 2003.

#### Submitted

U. Balachandran, B. Ma, B. L. Fisher, R. E. Koritala, D. J. Miller, H. Claus, P. Berghuis, B. W. Veal, V. K. Vlasko-Vlasov, U. Welp, and K. E. Gray, Fabrication of Coated Conductors by Inclined Substrate Deposition and Oxygen Doping of Grain Boundaries, Invited abstract to be presented at the 11<sup>th</sup> Intl. Workshop on Critical Currents in Superconductors, Tokyo, July 28-31, 2003.

#### **Patents: 2000-2003**

Fabrication of High Temperature Superconductors

Uthamalingam Balachandran, Stephen E. Dorris, , Beihai Ma, and Meiya Li

U.S. Patent No. 6,579,360 B2 (June 17, 2003).

Metallic Substrates for High-Temperature Superconductors

T. Truchan, D. Miller, K. C. Goretta, U. Balachandran, and R. Foley (U. of IL)

U.S. Patent No. 6,455,166 (Sept. 24, 2002).

Method for Preparing High-Temperature Superconductor

Uthamalingam Balachandran and Michael P. Chudzik

U.S. Patent No. 6,361,598 (March 26, 2002).

Shielded High- $T_c$  BSCCO Tapes or Wires for High-Field Applications

Uthamalingam Balachandran, Milan Lelovic, and Nicholas G. Eror

U.S. Patent No. 6,252,096 (June 26, 2001); U.S. Patent 6,466,805 (Oct. 15, 2002).

Thermomechanical Means to Improve Critical Current Density of BSCCO Tapes

Uthamalingam Balachandran, Roger B. Poeppel, Pradeep Haldar (IGC), and Lesizek

Motowidlo (IGC), U.S. Patent 6,240,619 (June 5, 2001).

Method of Manufacturing a High-Temperature Superconductor with Improved Transport Properties

Uthamalingam Balachandran, Richard Siegel, and Thomas Askew

U.S. Patent No. 6,191,075 (February 20, 2001).

Bearing Design for Flywheel Energy Storage Using High- $T_c$  Superconductors

John R. Hull and Thomas M. Mulcahy

U.S. Patent No. 6,153,958 (Nov. 28, 2000).

Method and Apparatus for Measuring Gravitational Acceleration Utilizing a High-Temperature Superconducting Bearing

John R. Hull

U.S. Patent 6,079,267 (June 27, 2000).

Improvements in Levitation Pressure and Friction Losses in Superconducting Bearings,

John R. Hull

U.S. Patent 6,175,175 (January 16, 2001).

Trapped Field Internal Dipole Superconducting Motor/Generator

John R. Hull

U.S. Patent 6,169,352 (January 2, 2001).

Reluctance Apparatus for Flywheel Energy Storage

John R. Hull

U.S. Patent 6,097,118 (August 1, 2000).

Large Area Bulk Superconductors

Dean J. Miller and Michael B. Field

U.S. Patent 6,410,487 (June 25, 2002).